

Streaming Tensor Train Approximation

Daniel Kressner¹, Bart Vandereycken², and Rik Voorhaar²

¹Institute of Mathematics, EPFL, CH-1015 Lausanne, Switzerland

²Section of Mathematics, University of Geneva, CH-1205 Geneva, Switzerland

Abstract

Tensor trains are a versatile tool to compress and work with high-dimensional data and functions. In this work we introduce the Streaming Tensor Train Approximation (STTA), a new class of algorithms for approximating a given tensor \mathcal{T} in the tensor train format. STTA accesses \mathcal{T} exclusively via two-sided random sketches of the original data, making it streamable and easy to implement in parallel – unlike existing deterministic and randomized tensor train approximations. This property also allows STTA to conveniently leverage structure in \mathcal{T} , such as sparsity and various low-rank tensor formats, as well as linear combinations thereof. When Gaussian random matrices are used for sketching, STTA is admissible to an analysis that builds and extends upon existing results on the generalized Nyström approximation for matrices. Our results show that STTA can be expected to attain a nearly optimal approximation error if the sizes of the sketches are suitably chosen. A range of numerical experiments illustrates the performance of STTA compared to existing deterministic and randomized approaches.

1 Introduction

This work proposes and analyzes a new randomized algorithm for compressing a tensor $\mathcal{T} \in \mathbb{R}^{n_1 \times n_2 \times \dots \times n_d}$ of order d in the so-called tensor train (TT) format [Oseledets, 2011]. The TT format (also called matrix product state – MPS – in physics [Schollwöck, 2011]) represents a tensor through contractions of third-order tensors, the so-called TT cores. Offering a number of key advantages, the TT format belongs to the most popular low-rank tensor formats. In particular, its multilinear structure and its close connection to low-rank matrix factorizations allow one to leverage tools from (numerical) linear algebra, such as the singular value decomposition (SVD), in the design and analysis of algorithms. During the last decade, the TT format has shown its utility in a wide variety of applications in scientific computing and data analysis; see [Grasedyck et al., 2013, Bachmayr et al., 2016, Khoromskij, 2018, Hackbusch, 2019, Uschmajew and Vandereycken, 2020] for an overview.

The randomized SVD, called the Halko–Martinson–Tropp (HMT) method [Halko et al., 2011] in the following, is a wildly popular method for obtaining a low-rank approximation to a matrix $A \in \mathbb{R}^{m \times n}$. It proceeds by first generating a (random) *dimension reduction matrix* (DRM) $X \in \mathbb{R}^{n \times r}$ with $r \ll n$. Then the product AX is computed and its columns are orthonormalized by a QR factorization, which we denote by $Q = \text{orth}(AX) \in \mathbb{R}^{n \times r}$. A low-rank approximation of A is obtained by setting $A \approx \hat{A}_{\text{HMT}} = Q(Q^\top A)$. While very simple and effective, the HMT method is not streamable in the sense of [Clarkson and Woodruff, 2009] since forming $Q^\top A$ requires two passes over the input data A . Although the sketch AX is linear in A , which makes it cheap to update when A undergoes a change of the form $A \rightarrow A + B$, this is no longer true for Q and $Q^\top A$. The generalized Nyström (GN) method, originally also devised in [Clarkson and Woodruff, 2009], mitigates this issue by performing a *two-sided* sketch. First, it generates two DRMs $X \in \mathbb{R}^{n \times r}$ and $Y \in \mathbb{R}^{m \times (r+\ell)}$ for some $\ell \geq 1$ such that $r + \ell \ll m$. After computing the sketches AX , $Y^\top A$, $Y^\top AX$, one obtains a low-rank approximation by setting

$$A \approx \hat{A}_{\text{GN}} := AX(Y^\top AX)^\dagger Y^\top A. \quad (1)$$

Here $(\cdot)^\dagger$ denotes the Moore–Penrose pseudoinverse by which multiplying is mathematically equivalent to solving a linear least-squares problem. As all three sketches are linear in A and they dominate the cost, the GN method is streamable. Moreover, the computation of the sketches can be carried out such that it requires only one pass over the data.

In this work, we present a streaming TT approximation (STTA) – an extension of the GN method to TTs. Our algorithm is streamable and requires only one pass over the data. Moreover, unlike most existing TT approximation methods, STTA parallelizes naturally with respect to the tensor modes, an attractive feature for high-order tensors. Note that the STTA method itself does not make any assumptions on the type of DRMs. For the case of Gaussian random DRMs, we will derive an upper bound on the expected error that generalizes

the matrix results from [Tropp et al., 2017, Nakatsukasa, 2020]. In particular, we prove that the expected error is quasi-optimal and close to the one obtained via TT-SVD using only moderate oversampling.

Several different randomized approaches for TT approximation have been proposed in the literature. A straightforward approach is to replace every truncated SVD inside the TT-SVD algorithm, the standard method for TT approximation [Oseledets, 2011], by the HMT method. This algorithm, called TT-HMT in the following, is analyzed for Gaussian random DRMs in [Huber et al., 2017, Wolf, 2019] and significant savings for a (very) sparse tensor \mathcal{T} are reported. In [Che and Wei, 2019], the TT-HMT method is presented as well, together with an adaptive variant. In [Alger et al., 2020], another approach is presented that is well suited for compressing high-order derivative tensors. This variant accesses the tensor through evaluations of the corresponding multilinear map and uses random Khatri–Rao product DRMs, that is, (columnwise) Khatri–Rao products of Gaussian random matrices instead of unstructured Gaussian random matrices.

Neither the TT-SVD algorithm nor any of the variants mentioned above is streamable or parallel in the modes; nestedness relations among the low-rank matrix factorizations constituting the TT format represent a major obstacle for doing so. The parallel streaming TT sketching (PSTT) algorithms described in [Shi et al., 2021] overcome this obstacle by first applying the HMT method to all relevant unfoldings of \mathcal{T} in parallel and restoring nestedness a posteriori, without losing any of the favorable approximation properties. The work by [Shi et al., 2021] also discusses the use of Khatri–Rao product DRMs and proposes variants that require only one pass over the input data \mathcal{T} . The PSTT algorithm and its variants inherit from the HMT method the need to compute (large) QR decompositions, which cannot be cheaply updated after a linear update of the data as explained above.

The work by [Daas et al., 2021] focuses on TT rounding, that is, the subsequent compression of a tensor that is already in TT format. The standard algorithm for TT rounding is essentially the TT-SVD and thus requires to first successively orthogonalize the TT cores of the input TT format, a costly step that prevents from attaining any significant savings when using the HMT method. An algorithm called “Randomize-then-Orthogonalize” in [Daas et al., 2021] circumvents this orthogonalization step by applying the HMT method to unfoldings of the full tensor and leveraging the TT format through the use of a TT DRM, that is, a TT with Gaussian random TT cores; see also [Ma and Solomonik, 2022]. A two-sided variant that uses the GN method with two TT DRMs instead of the HMT method is also presented. None of the algorithms presented in [Daas et al., 2021] are easy to parallelize with respect to the modes. Also, the formulation of the algorithms does not seem to allow for streaming and requires more than one pass over the input tensor.

The STTA method proposed in this work can be viewed as a streamable, two-sided variant of the PSST algorithm from [Shi et al., 2021]. Besides two-sided sketches of the input tensor, no other large-scale computation needs to be carried out in STTA. In particular, the QR decompositions of the PSST algorithm are avoided, which makes it cheaper to carry out updates, avoids the storage of large intermediate matrices, and allows one to easily exploit sparsity and other structure in the input tensor. As we will explain in Section 4.2, a particular combination of the STTA method with two TT DRMs becomes *mathematically* equivalent to the two-sided variant [Daas et al., 2021].

An important advantage of the one-pass nature of STTA is that it can be efficiently used to compress (or round) a structured tensor that is given in some data sparse format. For example, we explain in Section 4 in some detail the implementation for compressing Tucker, CP, and sparse tensors. Furthermore, thanks to its streamability, it is straightforward to apply STTA to a sum of all these different structures. We are not aware of an existing randomized method for which all these features have been highlighted.

1.1 Notation and preliminaries

We first recall important properties of the tensor train (TT) format that are needed throughout the paper. For more details and proofs, we refer to [Bachmayr et al., 2016, Hackbusch, 2019].

Given a matrix A or a tensor \mathcal{T} , its entries will be indexed as $[i_1, \dots, i_d]$. Furthermore, when an index i_μ is denoted as $:$, it represents all the entries for the μ th mode and will result in a slice of the matrix or tensor.

A tensor \mathcal{T} of size $n_1 \times n_2 \times \dots \times n_d$ is in the TT format if it can be written element-wise as

$$\mathcal{T}[i_1, \dots, i_d] = \sum_{\ell_1=1}^{r_1} \dots \sum_{\ell_{d-1}=1}^{r_{d-1}} C_1[1, i_1, \ell_1] C_2[\ell_1, i_2, \ell_2] \dots C_d[\ell_{d-1}, i_d, 1]. \quad (2)$$

The third-order tensors C_μ of size $r_{\mu-1} \times n_\mu \times r_\mu$ are the TT cores (where $r_0 = r_d = 1$). Using the matrix $C_\mu[:, i_\mu, :]$ of size $r_{\mu-1} \times r_\mu$, the relation (2) can be written compactly as a product of d matrices (where the first and last matrices collapse to a row and column vector, respectively) as follows:

$$\mathcal{T}[i_1, \dots, i_d] = C_1[1, i_1, :] C_2[:, i_2, :] \dots C_d[:, i_d, 1].$$

The generalized Nyström (GN) method uses two DRMs $X \in \mathbb{R}^{n \times r}$ and $Y \in \mathbb{R}^{m \times (r+\ell)}$, for some $\ell \geq 1$ such that $r + \ell < m$, to construct the approximation

$$\widehat{A}_{\text{GN}} = AX(Y^\top AX)^\dagger Y^\top A. \quad (8)$$

Again, this can be expressed in terms of a projection. Given two matrices B and C with the same number of rows, we define the *oblique projector* $\mathcal{P}_{B,C} = B(C^\top B)^\dagger C^\top$. It directly follows from (8) that

$$\widehat{A}_{\text{GN}} = \mathcal{P}_{AX,Y} A. \quad (9)$$

The fact that $\mathcal{P}_{AX,Y}$ is no longer orthogonal implies that the GN approximation is (slightly) worse than the HMT approximation for the same X . In terms of the expected error the following bound holds.

Theorem 2.1 ([Tropp et al., 2017, Theorem 4.3]). *Consider random Gaussian matrices X and Y of size $n \times r$ and $n \times (r + \ell)$, respectively, with $\ell > 0$. Then the expected approximation error of (8) is bounded by*

$$\mathbb{E} \|\widehat{A} - A\|_F^2 \leq \left(1 + \frac{r}{\ell - 1}\right) \left(1 + \frac{\widehat{r}}{r - \widehat{r} - 1}\right) \|A_{\widehat{r}} - A\|_F^2, \quad (10)$$

where $A_{\widehat{r}}$ is any best rank \widehat{r} approximation of A with $\widehat{r} < r - 1$.

Remark 2.2. *The formulation of Theorem 2.1 assumes that Y has more columns than X . Since*

$$\|(I - \mathcal{P}_{AX,Y})A\|_F = \|(I - \mathcal{P}_{AX,Y})A\|_F^\top = \|(I - \mathcal{P}_{A^\top Y,X})A^\top\|_F, \quad (11)$$

the bound (10) also holds in the reverse situation, that is, when X has size $n \times (r + \ell)$ and Y has size $n \times r$.

Let us emphasize again that the GN method is *streamable* and *one-pass*. It consists of two steps:

1. Sketch $AX, Y^\top A, Y^\top AX$.
2. Assemble $\widehat{A} = AX(Y^\top AX)^\dagger Y^\top A$.

The first step is linear in A , and the sketches are cheap to store or communicate if $r \ll \min(m, n)$. Moreover, this step typically dominates the overall computational effort, requiring $O(rmn)$ operations for dense matrices, whereas the second step only requires $O((r + \ell)r^2)$ operations; see [Nakatsukasa, 2020] for implementation aspects.

3 Streaming TT approximation (STTA)

We now explain our streamable TT approximation algorithm for a given tensor \mathcal{T} of size $n_1 \times \dots \times n_d$. The idea is to sketch every unfolding $\mathcal{T}^{\leq \mu} \in \mathbb{R}^{(n_1 \dots n_\mu) \times (n_{\mu+1} \dots n_d)}$ using several *dimension reduction matrices* (DRMs) X_μ, Y_μ of matching sizes:

$$\begin{aligned} X_\mu &\text{ is a 'right' DRM of size } (n_{\mu+1} \dots n_d) \times r_\mu^R \text{ for } 1 \leq \mu \leq d-1; \\ Y_\mu &\text{ is a 'left' DRM of size } (n_1 \dots n_\mu) \times r_\mu^L \text{ for } 1 \leq \mu \leq d-1. \end{aligned} \quad (12)$$

We require that either $r_\mu^R < r_\mu^L - 1$ for all μ or $r_\mu^L < r_\mu^R - 1$ for all μ . Our approximation will have TT rank $r_\mu := \min(r_\mu^L, r_\mu^R)$ for $\mu = 1, \dots, d-1$ and is obtained from the following sketches:

$$\begin{aligned} \Psi_\mu^L &= (Y_{\mu-1}^\top \otimes I) \mathcal{T}^{\leq \mu} X_\mu \text{ of size } (r_{\mu-1}^L n_\mu) \times r_\mu^R \text{ for } 1 \leq \mu \leq d; \\ \Omega_\mu &= Y_\mu^\top \mathcal{T}^{\leq \mu} X_\mu \text{ of size } r_\mu^L \times r_\mu^R \text{ for } 1 \leq \mu \leq d-1. \end{aligned} \quad (13)$$

For simplicity we use the convention that $Y_0 = X_d = 1$, so that (13) remains valid for $\mu = 1$ and $\mu = d$. Recall that Ψ_μ^L denotes the left unfolding of the $r_{\mu-1} \times n_\mu \times r_\mu^R$ tensor Ψ_μ . In terms of tensor diagrams, the relations (13) take the following form:

$$\begin{aligned} \begin{array}{c} r_{\mu-1}^L \quad \Psi_\mu^L \quad r_\mu^R \\ | \\ n_\mu \end{array} &:= \begin{array}{c} r_{\mu-1}^L \quad Y_{\mu-1} \quad \begin{array}{c} n_1 \\ \vdots \\ n_{\mu-1} \end{array} \quad \mathcal{T} \quad \begin{array}{c} n_{\mu+1} \\ \vdots \\ n_d \end{array} \quad X_\mu \quad r_\mu^R \\ | \\ n_\mu \end{array} \\ \\ \begin{array}{c} r_\mu^L \quad \Omega_\mu \quad r_\mu^R \\ | \\ n_\mu \end{array} &:= \begin{array}{c} r_\mu^L \quad Y_\mu \quad \begin{array}{c} n_1 \\ \vdots \\ n_\mu \end{array} \quad \mathcal{T} \quad \begin{array}{c} n_{\mu+1} \\ \vdots \\ n_d \end{array} \quad X_\mu \quad r_\mu^R \\ | \\ n_\mu \end{array} \end{aligned} \quad (14)$$

Using these sketches, we construct an approximation $\tilde{\mathcal{T}}$ as follows:

$$\tilde{\mathcal{T}} := \Psi_1 \overset{r_1^R}{\text{---}} \Omega_1^\dagger \overset{r_1^L}{\text{---}} \Psi_2 \overset{r_2^R}{\text{---}} \Omega_2^\dagger \overset{r_2^L}{\text{---}} \dots \overset{r_{d-1}^R}{\text{---}} \Omega_{d-1}^\dagger \overset{r_{d-1}^L}{\text{---}} \Psi_d \quad (15)$$

To arrive at a tensor diagram that takes the form of a TT as in (3), one needs to contract each Ω_μ^\dagger with an adjacent order-three tensor. When $r_\mu^R < r_\mu^L$, it is preferable to choose the tensor to the right, because otherwise the (representation) ranks are unnecessarily high. More specifically, we obtain a TT representation for $\tilde{\mathcal{T}}$ by defining each $r_{\mu-1}^R \times n_\mu \times r_\mu^R$ core C_μ via its right unfolding

$$C_\mu^R := \begin{cases} \Psi_1, & \mu = 1, \\ \Omega_{\mu-1}^\dagger \Psi_\mu, & \mu > 1. \end{cases} \quad (16)$$

Assuming that Ω_μ has full (column) rank, we can equivalently obtain C_μ^R as the solution of the linear least-squares problem

$$\min_X \|\Omega_{\mu-1} X - \Psi_\mu^R\|_F^2. \quad (17)$$

Especially when Ω_μ is not well-conditioned, care needs to be taken when solving this problem numerically; see also [Nakatsukasa, 2020, §4.1]. In our implementation, we use the LAPACK routine `gelsd` which utilizes a (truncated) SVD of $\Omega_{\mu-1}$ and discards singular values smaller than $\epsilon_{\text{mach}} \|\Omega_{\mu-1}\|_2$, where ϵ_{mach} denotes machine precision.

When $r_\mu^L > r_\mu^L$ it is preferable to contract Ω_μ^\dagger with the tensor on the left, that is, the TT core C_μ is an $r_{\mu-1}^L \times n_\mu \times r_\mu^L$ tensor defined via

$$C_\mu^L := \begin{cases} \Psi_\mu^L \Omega_\mu^\dagger, & \mu < d \\ \Psi_d, & \mu = d. \end{cases} \quad (18)$$

If Ω_μ has full row rank, this is equivalent to solving the linear least-squares problem $\min_X \|X \Omega_\mu - \Psi_\mu^L\|_F^2$.

Like the matrix case, our streaming tensor sketch algorithm (STTA) can be split into two subroutines. First we *sketch* the tensor \mathcal{T} , and then we *assemble* the TT from the sketches. These two routines are summarized below in Algorithms 3.1 and 3.2. For convenience we only state the version for $r_\mu^R < r_\mu^L$, which produces a TT of rank $(r_1^R, \dots, r_{d-1}^R)$; the other version is analogous.

Algorithm 3.1 STTA: sketch

Input: Tensor \mathcal{T} of shape $n_1 \times \dots \times n_d$; Right DRMs X_μ of shape $(n_{\mu+1} \dots n_d) \times r_\mu^R$ and left DRMs Y_μ of shape $(n_1 \dots n_\mu) \times r_\mu^L$ for $\mu = 1$ to $d-1$ with $r_\mu^R < r_\mu^L$.

Output: Sketches Ψ_μ of shape $r_{\mu-1}^L \times n_\mu \times r_\mu^R$ for $1 \leq \mu \leq d$; Sketches Ω_μ of shape $r_\mu^L \times r_\mu^R$ for $1 \leq \mu \leq d-1$.

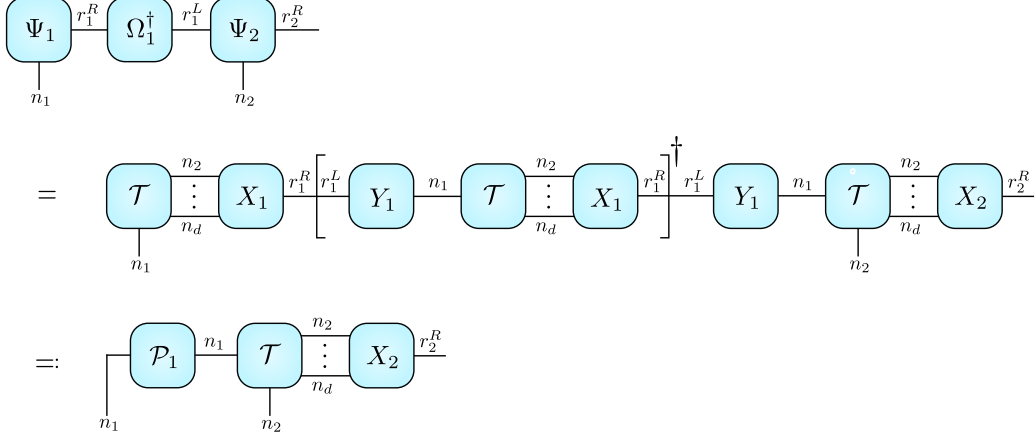
- 1: **for** $\mu = 1$ to d **do**
 - 2: $\mathcal{T}^{\leq \mu} \leftarrow \text{reshape}(\mathcal{T}, (n_1 \dots n_\mu) \times (n_{\mu+1} \dots n_d))$
 - 3: **if** $\mu = 1$ **then**
 - 4: $\Psi_1 \leftarrow \mathcal{T}^{\leq 1} X_1$
 - 5: **else if** $\mu < d$ **then**
 - 6: $\Psi_\mu \leftarrow (Y_{\mu-1}^\top \otimes I_{n_\mu}) \mathcal{T}^{\leq \mu} X_\mu$
 - 7: **else**
 - 8: $\Psi_d \leftarrow (Y_{d-1}^\top \otimes I_{n_d}) \mathcal{T}^{\leq d}$
 - 9: **end if**
 - 10: **if** $\mu < d$ **then**
 - 11: $\Omega_\mu \leftarrow Y_\mu^\top \mathcal{T}^{\leq \mu} X_\mu$
 - 12: **end if**
 - 13: **end for**
-

DRMs: Algorithm 3.2 takes $2d-2$ right and left DRMs as input. The simplest choice for DRMs are Gaussian random matrices, which lead to matrices X_μ and Y_μ that are independent with respect to μ . When \mathcal{T} is itself in low-rank format (TT, CP, and Tucker formats – see Sections 4.3 and 4.4), it is computationally advantageous to use a single TT DRM (a TT with Gaussian random TT cores) to define all right DRMs, and similarly for

To show (21), we first note that the definitions (13) and (20) imply

$$\left(\left[\Psi_1^L \Omega_1^\dagger \right] \otimes I \right) \Psi_2^L = \left(\left[\mathcal{T}^{\leq 1} X_1 (Y_1^\top \mathcal{T}^{\leq 1} X_1)^\dagger Y_1^\top \right] \otimes I \right) \mathcal{T}^{\leq 2} X_2 = (\mathcal{P}_1 \otimes I) \mathcal{T}^{\leq 2} X_2,$$

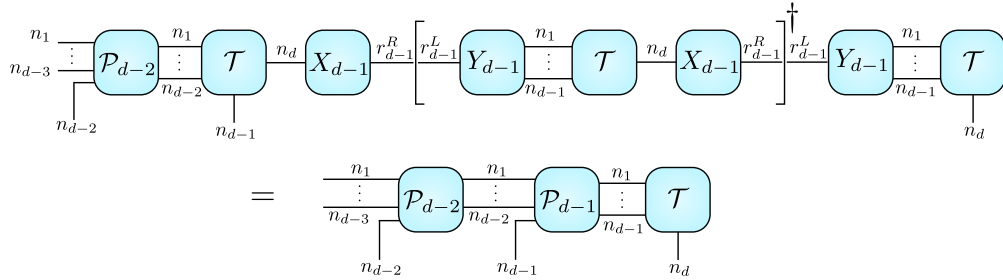
which corresponds to the diagram



Comparing with (15), this shows that the left part of the network representing $\tilde{\mathcal{T}}$ can be replaced by \mathcal{P}_1 . More generally, we have the relation

$$\left(\left[\mathcal{T}^{\leq \mu} X_\mu \Omega_\mu^\dagger \right] \otimes I \right) \Psi_{\mu+1}^L = \left(\left[\mathcal{T}^{\leq \mu} X_\mu (Y_\mu^\top \mathcal{T}^{\leq \mu} X_\mu)^\dagger Y_\mu^\top \right] \otimes I \right) \mathcal{T}^{\leq \mu+1} X_{\mu+1} = (\mathcal{P}_\mu \otimes I) \mathcal{T}^{\leq \mu+1} X_{\mu+1},$$

which allows us to successively replace, from the left to the right, the network representing $\tilde{\mathcal{T}}$ with the projectors \mathcal{P}_μ , until we arrive at



In turn, we obtain the network (22) as claimed.

Proposition 3.1. *The approximation $\tilde{\mathcal{T}}$ returned by STTA satisfies³*

$$\|\tilde{\mathcal{T}} - \mathcal{T}\|_F \leq \sum_{\mu=1}^{d-1} \left\| \prod_{\alpha < \mu} (\mathcal{P}_\alpha \otimes I) (I - \mathcal{P}_\mu) \mathcal{T}^{\leq \mu} \right\|_F. \quad (23)$$

Proof. Using (21), we have that

$$\begin{aligned} \|\mathcal{T} - \tilde{\mathcal{T}}\|_F &= \|[I - (\mathcal{P}_1 \otimes I) \cdots (\mathcal{P}_{d-2} \otimes I) \mathcal{P}_{d-1}] \mathcal{T}^{\leq d-1}\|_F \\ &\leq \|[I - (\mathcal{P}_1 \otimes I) \cdots (\mathcal{P}_{d-2} \otimes I)] \mathcal{T}^{\leq d-1}\|_F + \|(\mathcal{P}_1 \otimes I) \cdots (\mathcal{P}_{d-2} \otimes I) [I - \mathcal{P}_{d-1}] \mathcal{T}^{\leq d-1}\|_F. \end{aligned}$$

We can now continue the argument inductively since

$$\|[I - (\mathcal{P}_1 \otimes I) \cdots (\mathcal{P}_{d-2} \otimes I)] \mathcal{T}^{\leq d-1}\|_F = \|[I - (\mathcal{P}_1 \otimes I) \cdots \mathcal{P}_{d-2}] \mathcal{T}^{\leq d-2}\|_F. \quad \square$$

Gaussian DRMs. We now focus on the particular case when Gaussian DRMs X_μ, Y_μ are used and extend the bounds from Section 2 to the STTA algorithm.

³Note that the non-commuting product $\prod_{\alpha < \mu} (\mathcal{P}_\alpha \otimes I)$ in (23) is evaluated in natural increasing order with respect to α . Furthermore, for $\mu = 1$ the product is empty and corresponds to the identity matrix.

Theorem 3.2. *Suppose that the DRMs X_μ, Y_μ defined in (12) are independent standard Gaussian matrices with $r_\mu^R < r_\mu^L - 1$ and that the rank of $\mathcal{T}^{\leq \mu}$ is not smaller than r_μ^R for $\mu = 1, \dots, d-1$. Then for any $(\hat{r}_1, \dots, \hat{r}_{d-1})$ such that $\hat{r}_\mu < r_\mu^R - 1$, the STTA approximation $\tilde{\mathcal{T}}$ of \mathcal{T} obtained from Algorithm 3.2 satisfies*

$$\mathbb{E} \|\tilde{\mathcal{T}} - \mathcal{T}\|_F \leq \sum_{\mu=1}^{d-1} \left[\prod_{\alpha=1}^{\mu-1} c_\alpha \right] c'_\mu \sqrt{\sum_{k>\hat{r}_\mu} \sigma_k(\mathcal{T}^{\leq \mu})^2} \leq \left(\sum_{\mu=1}^{d-1} \left[\prod_{\alpha=1}^{\mu-1} c_\alpha \right] c'_\mu \right) \|\mathcal{T}_{\hat{\mathbf{r}}} - \mathcal{T}\|_F, \quad (24)$$

where $\mathcal{T}_{\hat{\mathbf{r}}}$ is any best TT approximation of \mathcal{T} of TT rank $(\hat{r}_1, \dots, \hat{r}_d)$, and c_μ, c'_μ are given by

$$c_\mu := 1 + \sqrt{\frac{r_\mu^R}{r_\mu^L - r_\mu^R - 1}}, \quad c'_\mu := \sqrt{1 + \frac{r_\mu^R}{r_\mu^L - r_\mu^R - 1}} \cdot \sqrt{1 + \frac{\hat{r}_\mu}{r_\mu^R - \hat{r}_\mu - 1}}. \quad (25)$$

Proof. By the assumptions, both $\mathcal{T}^{\leq \mu} X_\mu$ and $Y_\mu^\top \mathcal{T}^{\leq \mu} X_\mu$ have full column rank almost surely. We consider arbitrary $1 \leq \mu < d-1$ and temporarily consider X_μ fixed (such that the full-rank condition holds). The QR decomposition $\mathcal{T}^{\leq \mu} X_\mu = QR$ yields an invertible factor R of size $r_\mu^R \times r_\mu^R$, which allows us to rewrite the definition (20) of \mathcal{P}_μ as follows:

$$\mathcal{P}_\mu = \mathcal{T}^{\leq \mu} X_\mu (Y_\mu^\top \mathcal{T}^{\leq \mu} X_\mu)^\dagger Y_\mu^\top = QR (Y_\mu^\top QR)^\dagger Y_\mu^\top = Q (Y_\mu^\top Q)^\dagger Y_\mu^\top.$$

We now complete the r_μ^R columns of Q to a square orthogonal matrix $[Q \quad Q_\perp]$. Using $QQ^\top + Q_\perp Q_\perp^\top = I$ we obtain for any matrix A of size $(n_1 \cdots n_\mu) \times (n_{\mu+1} \cdots n_d)$ that

$$\begin{aligned} \|\mathcal{P}_\mu A\|_F &\leq \|(Y_\mu^\top Q)^\dagger Y_\mu^\top Q Q^\top A\|_F + \|(Y_\mu^\top Q)^\dagger Y_\mu^\top Q_\perp Q_\perp^\top A\|_F \\ &= \|Q^\top A\|_F + \|(Y_\mu^\top Q)^\dagger Y_\mu^\top Q_\perp Q_\perp^\top A\|_F \leq \|A\|_F + \|(Y_\mu^\top Q)^\dagger Y_\mu^\top Q_\perp Q_\perp^\top A\|_F. \end{aligned}$$

By the orthogonal invariance of Gaussian random matrices, $Z_1 := Y_\mu^\top Q$ and $Z_2 := Y_\mu^\top Q_\perp$ are independent Gaussian random matrices of size $r_\mu^L \times r_\mu^R$ and $r_\mu^L \times (n_1 \cdots n_\mu - r_\mu^R)$, respectively. This allows us to apply Propositions 10.1 and 10.2 from [Halko et al., 2011] to obtain

$$\mathbb{E}_{Z_1, Z_2} \|Z_1^\dagger Z_2 Q_\perp^\top A\|_F \leq \sqrt{\mathbb{E}_{Z_1, Z_2} \|Z_1^\dagger Z_2 Q_\perp^\top A\|_F^2} = \sqrt{\mathbb{E}_{Z_1} \|Z_1^\dagger\|_F^2} \|Q_\perp^\top A\|_F = \sqrt{\frac{r_\mu^R}{r_\mu^L - r_\mu^R - 1}} \|Q_\perp^\top A\|_F.$$

In summary, we have

$$\mathbb{E}_{X_1, Y_1} \|\mathcal{P}_\mu A\|_F \leq c_\mu \|A\|_F.$$

Now, by the law of total expectation, it holds that

$$\begin{aligned} \mathbb{E}_{X_\mu, Y_\mu, \dots, X_\mu, Y_\mu} \|\prod_{\alpha=1}^{\mu-1} (\mathcal{P}_\alpha \otimes I) (I - \mathcal{P}_\mu) \mathcal{T}^{\leq \mu}\|_F \\ &= \mathbb{E}_{X_2, Y_2, \dots, X_\mu, Y_\mu} \left[\mathbb{E}_{X_1, Y_1} \|(\mathcal{P}_1 \otimes I) \prod_{\alpha=2}^{\mu-1} (\mathcal{P}_\alpha \otimes I) (I - \mathcal{P}_\mu) \mathcal{T}^{\leq \mu}\|_F \mid X_2, Y_2, \dots, Y_\mu, X_\mu \right] \\ &\leq c_1 \mathbb{E}_{X_2, Y_2, \dots, X_\mu, Y_\mu} \left[\|\prod_{\alpha=2}^{\mu-1} (\mathcal{P}_\alpha \otimes I) (I - \mathcal{P}_\mu) \mathcal{T}^{\leq \mu}\|_F \right], \end{aligned}$$

where we used that only \mathcal{P}_1 depends on X_1, Y_1 . Continuing inductively we obtain

$$\mathbb{E}_{X_1, Y_1, \dots, X_\mu, Y_\mu} \|\prod_{\alpha=1}^{\mu-1} (\mathcal{P}_\alpha \otimes I) (I - \mathcal{P}_\mu) \mathcal{T}^{\leq \mu}\|_F \leq c_1 \cdots c_{\mu-1} \mathbb{E}_{X_\mu, Y_\mu} \|(I - \mathcal{P}_\mu) \mathcal{T}^{\leq \mu}\|_F. \quad (26)$$

The last factor coincides with the GN approximation error, which – according to Theorem 2.1 – is bounded by

$$\begin{aligned} \mathbb{E}_{X_\mu, Y_\mu} \|(I - \mathcal{P}_\mu) \mathcal{T}^{\leq \mu}\|_F^2 &\leq \left(1 + \frac{r_\mu^R}{r_\mu^L - r_\mu^R - 1} \right) \left(1 + \frac{\hat{r}_\mu}{r_\mu^R - \hat{r}_\mu - 1} \right) \sum_{k>\hat{r}_\mu} \sigma_k(\mathcal{T}^{\leq \mu})^2 \\ &= (c'_\mu)^2 \sum_{k>\hat{r}_\mu} \sigma_k(\mathcal{T}^{\leq \mu})^2 \end{aligned}$$

for any $\hat{r}_\mu < r_\mu^R - 1$, where $\sigma_k(\cdot)$ denotes the k th largest singular value of a matrix. Finally, we apply Proposition 3.1 to obtain the first inequality of (24). The second inequality follows directly from the general bound

$$\sum_{k>\hat{r}_\mu} \sigma_k(\mathcal{T}^{\leq \mu})^2 \leq \|\mathcal{T} - \mathcal{T}_{\hat{\mathbf{r}}}\|_F^2; \quad (27)$$

see, e.g., [Hackbusch, 2019, Thm. 11.6]. \square

Observe that if one uses $r_\mu^L = \kappa r_\mu^R$ for a constant $\kappa > 1$ in Theorem 3.2, then $c_\mu = O(1)$. As κ increases, c_μ approaches one, which mitigates the exponential dependence on d in the constants.

The condition $r_\mu^R < r_\mu^L - 1$ for all μ of Theorem 3.2 can be replaced by $r_\mu^L < r_\mu^R - 1$, using a modification of the proof that proceeds in the other direction, from ‘right to left’. The approximation bound (24) still holds but with the roles of r_μ^R and r_μ^L reversed in (25).

Random TT DRMs. The proof of Theorem 3.2 heavily relies on the DRMs being Gaussian. As mentioned before and demonstrated in [Daas et al., 2021, Ma and Solomonik, 2022], it can often be computationally beneficial to use TT DRMs, for which we now give a formal definition.

Definition 3.3 (TT DRM). *Consider a tensor in TT format with random TT cores $C_\mu \in \mathbb{R}^{r_{\mu-1}^{r_\mu^L} \times n_\mu \times r_\mu^L}$ for which the entries are i.i.d. normal random variables with zero mean and variance $1/r_\mu^L$. Then left TT DRMs (Y_1, \dots, Y_{d-1}) , required as input by Algorithm 3.1, are defined via the (left) interface matrices*

$$Y_\mu := C_{\leq \mu} \in \mathbb{R}^{(n_1 \cdots n_\mu) \times r_\mu}, \quad \mu = 1, \dots, d-1,$$

which satisfy the nestedness relations (4), that is, $Y_\mu = (Y_{\mu-1} \otimes I)C_\mu^L$.

Analogously, right TT DRMs (X_1, \dots, X_{d-1}) are defined through $X_\mu := C_{> \mu}$ for another (independent) set of random TT cores $C_\mu \in \mathbb{R}^{r_{\mu-1}^R \times n_\mu \times r_\mu^R}$ with variance $1/r_{\mu-1}^R$.

The normalization of the variance in Definition 3.3 is chosen so that we have $\mathbb{E} \|XC_\mu^L\|_F^2 = \|X\|_F^2$ for each TT core C_μ and any fixed matrix X of appropriate size. This avoids numerical difficulties, such as over- or underflow, in particular when dealing with tensors of high order as in Section 5.7.

Proving an analogue to Theorem 3.2 for TT DRMs is difficult. As a first, preliminary result, we prove that the product $\mathcal{P} = (\mathcal{P}_1 \otimes I) \cdots (\mathcal{P}_{d-2} \otimes I) \mathcal{P}_{d-1}$, which produces the STTA approximation $\tilde{\mathcal{T}} = \mathcal{P}\mathcal{T}$, is itself an oblique projector. This intriguing property does not hold for Gaussian DRMs.

Lemma 3.4. *Suppose that $r_\mu^R \geq r_\mu^L$ for all μ , and (Y_1, \dots, Y_{d-1}) is a left TT DRM. If $\text{rank}(\mathcal{T}^{\leq \mu}) \geq r_\mu^R$ for all μ , then $\mathcal{P} := (\mathcal{P}_1 \otimes I) \cdots (\mathcal{P}_{d-2} \otimes I) \mathcal{P}_{d-1}$ is an oblique projector almost surely.*

Proof. We first establish $Y_\mu(\mathcal{P}_{\mu-1} \otimes I) = Y_\mu$ from the nestedness relations (4):

$$\begin{aligned} Y_\mu^\top (\mathcal{P}_{\mu-1} \otimes I) &= (C_\mu^L)^\top (Y_{\mu-1}^\top \otimes I) [\mathcal{T}^{\leq \mu-1} X_{\mu-1} (Y_{\mu-1}^\top \mathcal{T}^{\leq \mu-1} X_{\mu-1})^\dagger Y_{\mu-1}^\top \otimes I] \\ &= (C_\mu^L)^\top [Y_{\mu-1}^\top \mathcal{T}^{\leq \mu-1} X_{\mu-1} (Y_{\mu-1}^\top \mathcal{T}^{\leq \mu-1} X_{\mu-1})^\dagger Y_{\mu-1}^\top \otimes I] \\ &= (C_\mu^L)^\top (Y_{\mu-1}^\top \otimes I) = Y_\mu^\top. \end{aligned}$$

Here, we used that the $r_\mu^L \times r_\mu^R$ matrix $Y_{\mu-1}^\top \mathcal{T}^{\leq \mu-1} X_{\mu-1}$ has full row rank almost surely because of $r_\mu^R \geq r_\mu^L$. It now follows that

$$\mathcal{P}_\mu (\mathcal{P}_{\mu-1} \otimes I) = \mathcal{T}^{\leq \mu} X_\mu \Omega_\mu^\dagger Y_\mu^\top (\mathcal{P}_{\mu-1} \otimes I) = \mathcal{T}^{\leq \mu} X_\mu \Omega_\mu^\dagger Y_\mu^\top = \mathcal{P}_\mu. \quad (28)$$

We now show that $(\mathcal{P}_1 \otimes I) \cdots (\mathcal{P}_{d-2} \otimes I) \mathcal{P}_{d-1}$ is a projector. For convenience, we omit writing the $\otimes I$ factors. Observe that by applying (28) multiple times, we get the identities

$$\mathcal{P}_\mu \cdots \mathcal{P}_2 \mathcal{P}_1 = \mathcal{P}_\mu \cdots \mathcal{P}_3 \mathcal{P}_2 = \cdots = \mathcal{P}_\mu$$

and

$$(\mathcal{P}_\mu \cdots \mathcal{P}_2 \mathcal{P}_1) (\mathcal{P}_1 \mathcal{P}_2 \cdots \mathcal{P}_\mu) = \mathcal{P}_\mu \cdots \mathcal{P}_2 \mathcal{P}_1 \mathcal{P}_2 \cdots \mathcal{P}_\mu = \mathcal{P}_\mu \cdots \mathcal{P}_3 \mathcal{P}_2 \mathcal{P}_3 \cdots \mathcal{P}_\mu = \cdots = \mathcal{P}_\mu,$$

which allow us to show that

$$(\mathcal{P}_1 \cdots \mathcal{P}_\mu) (\mathcal{P}_1 \cdots \mathcal{P}_\mu) = (\mathcal{P}_1 \cdots \mathcal{P}_\mu) (\mathcal{P}_\mu \cdots \mathcal{P}_1) (\mathcal{P}_1 \cdots \mathcal{P}_\mu) = (\mathcal{P}_1 \cdots \mathcal{P}_\mu),$$

as required. \square

The assumption $r_\mu^R \geq r_\mu^L$ can be replaced by $r_\mu^L \geq r_\mu^R$. In this case, the STTA approximation satisfies $\tilde{\mathcal{T}} = \mathcal{P}\mathcal{T}$ for an oblique projector \mathcal{P} associated with right TT DRMs (X_1, \dots, X_{d-1}) .

4 Sketching structured tensors

We recall that STTA requires the sketches Ψ_μ, Ω_μ defined in (14). For a general order- d tensor $\mathcal{T} \in \mathbb{R}^{n_1 \times \dots \times n_d}$, the straightforward computation of these sketches requires a cost of $O(dn^d)$, which becomes excessive for large d . On the other hand, large-scale tensors usually have some *structure* that allows for faster sketching. In this section, we will explain how the STTA algorithm can be efficiently implemented for tensors with the following structures:

- sparse tensors;
- TT tensors (recompression);
- CP tensors;
- Tucker tensors.

Among these, only sparse tensors can be efficiently sketched using Gaussian DRMs; for the other formats we will instead use TT DRMs for sketching. Although our error bounds only apply to Gaussian DRMs, we will see that TT DRMs deliver similar performance.

Because of the linearity of sketching, we automatically obtain efficient algorithms for approximating linear combinations of any of these types of structured tensors. For example, one might be interested in sketching a sum of a sparse tensor and a TT.

4.1 Sketching sparse tensors

Suppose we want to approximate an $n_1 \times \dots \times n_d$ sparse tensor \mathcal{T} with $N \ll n_1 \dots n_d$ nonzero entries. These entries are represented via a list $\mathcal{E} = (\mathcal{E}_1, \dots, \mathcal{E}_N) \in \mathbb{R}^N$ of values and a list \mathcal{J} of N multi-indices $(i_j^{(1)}, \dots, i_j^{(d)})$, with $1 \leq i_j^{(\mu)} \leq n_\mu$ and $1 \leq j \leq N$. Given arbitrary DRMs X_μ, Y_μ , the sketches Ω_μ, Ψ_μ can be computed entry-wise as follows:

$$\Omega_\mu[k, l] = (Y_\mu^\top \mathcal{T}^{\leq \mu} X_\mu)[k, l] = \sum_{j=1}^N \mathcal{E}_j Y_\mu \left[i_j^{(1)}, \dots, i_j^{(\mu)}, k \right] X_\mu \left[i_j^{(\mu+1)}, \dots, i_j^{(d)}, l \right] \quad (29)$$

$$\Psi_\mu[k, l, m] = ((Y_{\mu-1}^\top \otimes I) \mathcal{T}^{\leq \mu} X_\mu)[k, l, m] = \sum_{\substack{j=1 \\ i_j^{(\mu)}=l}}^N \mathcal{E}_j Y_{\mu-1} \left[i_j^{(1)}, \dots, i_j^{(\mu-1)}, k \right] X_\mu \left[i_j^{(\mu+1)}, \dots, i_j^{(d)}, m \right]. \quad (30)$$

Note that we tacitly reshaped Y_μ into an $n_1 \times \dots \times n_\mu \times r_\mu^L$ tensor in order to access its rows by the multi-index $(i_j^{(1)}, \dots, i_j^{(\mu)})$, and similarly for X_μ and $Y_{\mu-1}$. Furthermore, Ψ_μ is viewed as a $r_{\mu-1}^L \times n_\mu \times r_\mu^R$ tensor.

Gaussian DRMs. For larger d and modest N , most rows of Y_μ and X_μ are never needed in (29). This allows us to efficiently use Gaussian DRMs in this context if we only generate those rows of X_μ and Y_μ that will actually be accessed. In order to do this in a distributed setting, we need to generate rows of a DRM *on demand* and *consistently* for each mode μ . One such way is to use a simple hashing algorithm to convert the indices $(i_j^{(1)}, \dots, i_j^{(\mu)})$ indexing the row of the DRM into a pseudorandom integer, which is then cast into a floating point number between 0 and 1, and finally converted into a normally distributed number. In the context of sketching this seems to produce pseudorandom numbers that are as good as those generated by more advanced pseudorandom number generators.

The formal procedure is detailed below in Algorithm 4.1. The seed s is specific to each mode μ and ensures that the entries of X_μ (or Y_μ) are consistent in a distributed setting. The uniform numbers are converted to normally distributed numbers by applying the inverse CDF. For the hashing function, we used `splitmix64` which generates adequate pseudo-random numbers.⁴

Using Algorithm 4.1 we only generate *at most* N rows of each DRM, requiring a total cost of $O(Nrd)$ to generate all DRMs. The asymptotic cost of computing Ω_μ using (29) is therefore $O(Nr^2)$ flops. Computing Ψ_μ using (30) has the same cost. This gives a total asymptotic cost for all the sketches with Gaussian DRMs of $O(Nr^2d)$, with straightforward parallelization with respect to the number of nonzero entries N .

⁴See https://rosettacode.org/wiki/Pseudo-random_numbers/Splitmix64 and <https://docs.oracle.com/javase/8/docs/api/java/util/SplittableRandom.html>.

⁵We first set the leftmost 3 bits of h_j to 001 to avoid NaN/infinite flags, and ensure a nonzero exponent. This does not affect the mantissa. Recall that the mantissa of a floating point number with nonzero exponent lies in the interval $[0.5, 1]$.

Algorithm 4.1 Hashed pseudorandom number generator that returns one row of a Gaussian DRM.

Input: Indices (i_1, \dots, i_μ) and integers (n_1, \dots, n_μ) such that $1 \leq i_j \leq n_j$, integer $r \geq 1$, seed s .

Output: (x_1, \dots, x_r) pseudorandom numbers with i.i.d. normal distribution

```

1:  $m \leftarrow 0$ 
2: for  $j = 1$  to  $\mu$  do
3:    $m \leftarrow n_j(m + i_j)$  // Turn multi-index into linear index
4: end for
5:  $m \leftarrow mr + \text{hash}(s)$ 
6: for  $j = 1$  to  $r$  do
7:    $h_j \leftarrow \text{hash}(m + j)$  // hash produces unsigned integers
8:    $x_j \leftarrow$  Interpret  $h_j$  as floating point number5 and extract mantissa.
9:    $x_j \leftarrow 2x_j - 1$ .
10:   $x_j \leftarrow \text{normal\_inverse\_cdf}(x_j)$  // Apply inverse CDF of the normal distribution
11: end for

```

TT DRMs. TT DRMs can also be used to efficiently sketch sparse tensors. This is because of the nestedness relations (4), which allow us to efficiently retrieve the entries with indices $[i_j^{(1)}, \dots, i_j^{(\mu)}, k]$ of the left interface matrices $C^{\leq \mu}$ subsequently for $\mu = 1, \dots, d$. Algorithm 4.2 describes the resulting procedure. This allows us to compute within $O(Nr^2d)$ operations all the entries of the TT DRMs Y_μ and X_μ needed for sketching in one sweep for all μ . With these entries at hand, we can sketch with TT DRMs using (29) and (30) at the same asymptotic cost as when sketching with Gaussian DRMs.

Algorithm 4.2 Selected entries of left interface matrices for a TT

Input: Tensor train cores C_1, \dots, C_d with each C_μ of size $r_{\mu-1} \times n_\mu \times r_\mu$;

List of indices $\mathcal{J} = \{(i_1^{(1)}, \dots, i_1^{(d)}), \dots, (i_N^{(1)}, \dots, i_N^{(d)})\}$.

Output: Matrices V_1, \dots, V_d of sizes $N \times r_\mu$ with entries of left interface matrices $C^{\leq \mu}$ corresponding to \mathcal{J} .

```

1:  $V_1 \leftarrow \mathbf{0}_{N \times r_1}$ 
2: for  $j = 1$  to  $N$  do
3:    $V_1[j, :] \leftarrow C_1[1, i_j^{(1)}, :]$ 
4: end for
5: for  $\mu = 2$  to  $d$  do
6:    $V_\mu \leftarrow \mathbf{0}_{N \times r_\mu}$ 
7:   for  $\ell = 1$  to  $n_\mu$  do
8:      $M \leftarrow C_\mu[:, \ell, :]$ 
9:     for  $j = 1$  to  $N$  such that  $i_j^{(\mu)} = \ell$  do
10:       $V_\mu[j, :] \leftarrow V_{\mu-1}[j, :]M$ 
11:    end for
12:  end for
13: end for

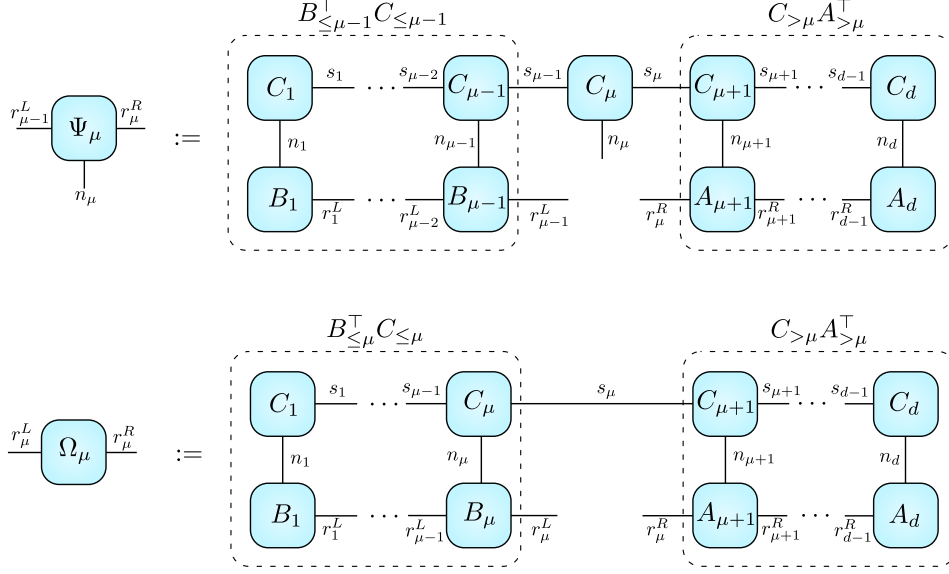
```

4.2 Sketching tensor trains

Let us now consider a tensor \mathcal{T} in TT format with a relatively high TT rank (s_1, \dots, s_{d-1}) , which we aim to compress to lower TT rank (r_1, \dots, r_{d-1}) , that is, $r_\mu < s_\mu$. It is clear that Gaussian DRMs are not well suited for this purpose simply because all entries of the DRMs need to be accessed at least once during the sketch computation, yielding a complexity of at least $O(n^d)$ for computing the sketches. On the other hand, we will see that sketching with TT DRMs yields a computational cost that is linear in d (assuming fixed TT ranks).

Let B_μ denote the cores of a random TT of TT rank $(r_1^L, \dots, r_{d-1}^L)$ that defines a left TT DRM (Y_1, \dots, Y_{d-1}) according to Definition 3.3. Similarly, let A_μ denote the cores of a random TT of TT rank $(r_1^R, \dots, r_{d-1}^R)$ that defines a right TT DRM (X_1, \dots, X_{d-1}) . Denoting the cores of \mathcal{T} by C_μ and inserting the TT diagrams for

$X_\mu, Y_\mu, \mathcal{T}$ into the tensor diagrams (14), we obtain the following diagrams for Ψ_μ and Ω_μ :



Let $r = \max_\mu(r_\mu^L, r_\mu^R)$ and $s = \max_\mu s_\mu$. All the products $B_{\leq\mu}^\top C_{\leq\mu}$ and $C_{>\mu} A_{>\mu}^\top$ (indicated by boxes above) can be computed efficiently for every $1 \leq \mu \leq d-1$ in a single sweep, at a total cost of $O(rs^2nd)$ flops. Given $B_{\leq\mu}^\top C_{\leq\mu}$ and $C_{>\mu} A_{>\mu}^\top$, we can compute each Ψ_μ at a cost of $O(rs^2n)$ flops, and Ω_μ at a cost of $O(r^2s)$ flops. This gives a total complexity of $O(rs^2nd)$ for sketching a TT using TT DRMs. The procedure is summarized in Algorithm 4.3, an efficient implementation of Algorithm 3.1 when TT DRMs are used to sketch a TT tensor \mathcal{T} .

Algorithm 4.3 STTA: sketch a TT tensor with TT DRMs

Input: TT to be sketched with cores C_1, \dots, C_d ; Left TT DRM with cores B_1, \dots, B_d ;

Right TT DRM with cores A_1, \dots, A_d .

Output: Sketches Ψ_1, \dots, Ψ_d , and $\Omega_1, \dots, \Omega_{d-1}$.

- 1: $L_1 \leftarrow B_1^\top C_1$
 - 2: **for** $\mu = 2$ to $d-1$ **do**
 - 3: $L_\mu[:, :] \leftarrow \sum_{ijk} L_{\mu-1}[i, j] B_\mu[i, k, :] C_\mu[j, k, :]$
 - 4: **end for**
 - 5: $R_{d-1} \leftarrow C_d A_d^\top$
 - 6: **for** $\mu = d-2$ to 2 **do**
 - 7: $R_\mu[:, :] \leftarrow \sum_{ijk} R_{\mu+1}[i, j] C_{\mu+1}[:, k, i] A_{\mu+1}[:, k, j]$
 - 8: **end for**
 - 9: **for** $\mu = 1$ to $d-1$ **do**
 - 10: $\Omega_\mu \leftarrow L_\mu R_\mu$
 - 11: **end for**
 - 12: $\Psi_1 \leftarrow C_1 R_1$
 - 13: **for** $\mu = 2$ to $d-1$ **do**
 - 14: $\Psi_\mu[:, :, :] \leftarrow \sum_{ij} L_\mu[:, i] C_\mu[i, :, j] R_\mu[j, :, :]$
 - 15: **end for**
 - 16: $\Psi_d \leftarrow L_d C_d$
-

We remark that Algorithm 4.3 can be adapted for sketching matrix product operators (MPO) [Orús, 2014], an extension of the TT format to linear operators. This is because an MPO can be transformed into a TT through reshaping its cores.

Remark 4.1. Algorithm 4.3 partly reproduces the two-sided method, Algorithm 3.3, from [Daas et al., 2021]. In particular, both algorithms compute the matrices $L_\mu = B_{\leq\mu}^\top C_{\leq\mu}$ and $R_\mu = C_{>\mu} A_{>\mu}^\top$ in the same fashion. There are however also differences. In the notation of this paper, Algorithm 3.3 from [Daas et al., 2021] computes a factored pseudo-inverse of $\Omega_\mu = L_\mu R_\mu$ and then uses these factors to compress the cores C_μ of the input tensor. This last step has the same complexity as the overall algorithm; it is however not linear in C_μ and thus not streamable. While mathematically equivalent, our algorithms (Algorithm 4.3 combined with Algorithm 3.2) avoid the explicit computation of the factored pseudo-inverse. Through the use of Ψ_μ , the majority of the computation

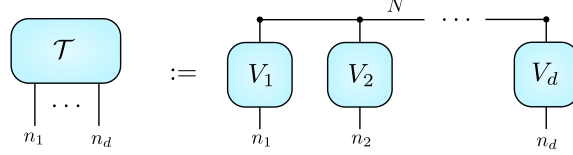
(Algorithm 4.3) is linear in each C_μ and thus streamable. Algorithm 3.2 also does not involve the (potentially large) cores of the input tensor.

4.3 Sketching canonical polyadic decompositions

The canonical polyadic (CP) decomposition [Kolda and Bader, 2009] represents a tensor \mathcal{T} as a sum of N rank-1 tensors. The CP decomposition can be expressed in terms of factor matrices $V_1 \in \mathbb{R}^{N \times n_1}, \dots, V_d \in \mathbb{R}^{N \times n_d}$ as follows:

$$\mathcal{T} = \sum_{i=1}^N V_1[i, :] \otimes V_2[i, :] \otimes \dots \otimes V_d[i, :]. \quad (31)$$

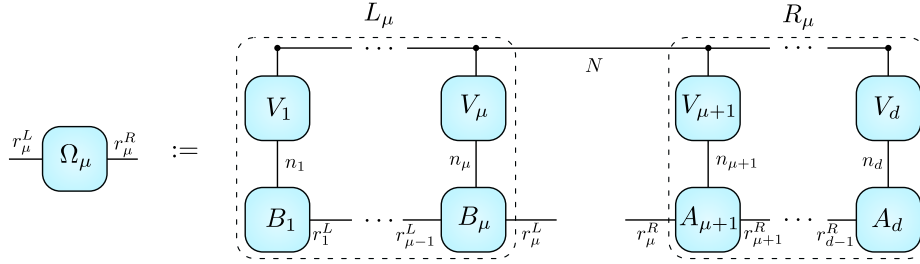
The tensor diagram corresponding to this equation is given by



As in the TT case, sketching \mathcal{T} with Gaussian DRMs would be too expensive and we therefore resort again to left/right TT DRMs with cores A_1, \dots, A_d and B_1, \dots, B_d , respectively. The sketch $\Omega_\mu = Y_\mu^\top \mathcal{T}^{\leq \mu} X_\mu$ is obtained from

$$\Omega_\mu = L_\mu R_\mu := [B_{\leq \mu}^\top (V_1 \odot \dots \odot V_\mu)^\top] [(V_{\mu+1} \odot \dots \odot V_d) A_{> \mu}^\top], \quad (32)$$

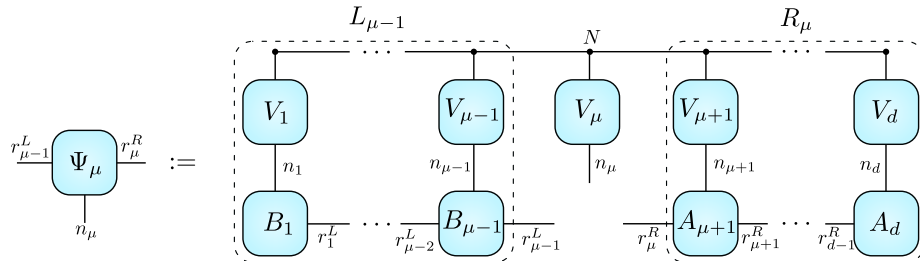
where \odot denotes the row-wise Khatri-Rao product, that is, $V_\mu \odot V_{\mu+1}$ is the $N \times n_\mu n_{\mu+1}$ matrix that contains in the i th row all products $V_\mu[i_1, i_2] V_{\mu+1}[i_1, i_3]$. The relation (32) in terms of diagrams:



Similarly we obtain the sketch Ψ_μ using the following contraction

$$\Psi_\mu[i_1, i_2, i_3] = \sum_j L_{\mu-1}[i_1, j] V_\mu[j, i_2] R_\mu[j, i_3], \quad (33)$$

or in terms of diagrams:



The matrices L_μ and R_μ can be efficiently computed in a single sweep for all $1 \leq \mu \leq d$ at a total cost of $O(Nnr^2d)$ flops. Given L_μ and R_μ , then Ω_μ can be computed at a cost of $O(Nr^2)$ flops, and Ψ_μ at a cost of $O(Nnr^2)$ flops. This gives a total cost of $O(Nnr^2d)$ to sketch a CP tensor using TT DRMs. The procedure is summarized in Algorithm 4.4.

Algorithm 4.4 STTA: sketch a tensor in CP decomposition with TT DRMs

Input: CP to be sketched with factor matrices V_1, \dots, V_d , left TT DRM with cores B_1, \dots, B_d , right TT DRM with cores A_1, \dots, A_d .

Output: Sketches Ψ_1, \dots, Ψ_d and $\Omega_1, \dots, \Omega_{d-1}$.

- 1: $L_1 \leftarrow B_1^\top V_1^\top$
 - 2: **for** $\mu = 2$ to $d - 1$ **do**
 - 3: $L_\mu[i_1, i_2] \leftarrow \sum_{j_1, j_2} L_{\mu-1}[j_1, i_2] V_\mu[i_2, j_2] B_\mu[j_1, j_2, i_1]$
 - 4: **end for**
 - 5: $R_{d-1} \leftarrow V_d A_d^\top$
 - 6: **for** $\mu = d - 2$ to 2 **do**
 - 7: $R_\mu[i_1, i_2] \leftarrow \sum_{j_1, j_2} R_{\mu+1}[i_1, j_1] V_{\mu+1}[i_1, j_2] B_{\mu+1}[i_2, j_2, j_1]$
 - 8: **end for**
 - 9: **for** $\mu = 1$ to $d - 1$ **do**
 - 10: $\Omega_\mu \leftarrow L_\mu R_\mu$
 - 11: **end for**
 - 12: $\Psi_1[1, i_1, i_2] \leftarrow \sum_j V_1[j, i_1] R[j, i_2]$
 - 13: **for** $\mu = 2$ to $d - 2$ **do**
 - 14: $\Psi_\mu[i_1, i_2, i_3] = \sum_j L_{\mu-1}[i_1, j] V_\mu[j, i_2] R_\mu[j, i_3]$
 - 15: **end for**
 - 16: $\Psi_d[i_1, i_2, 1] \leftarrow \sum_j V_d[j, i_1] R_\mu[j, i_2]$.
-

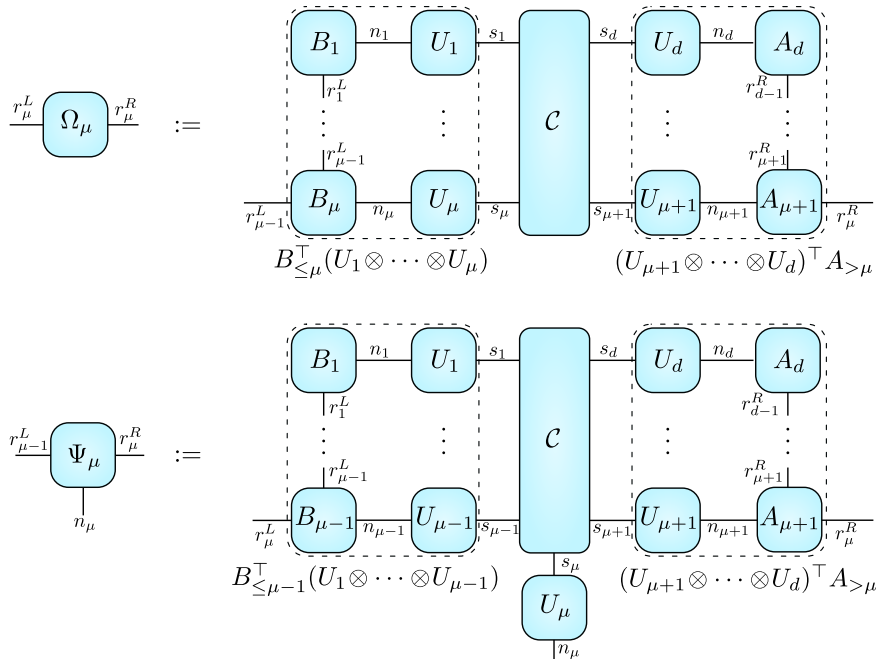
4.4 Sketching Tucker decomposition

The Tucker decomposition [Kolda and Bader, 2009] represents a tensor \mathcal{T} of size $n_1 \times \dots \times n_d$ by a core tensor \mathcal{C} of (usually smaller) size $s_1 \times \dots \times s_d$ multiplied in each mode by a factor matrix $U_\mu \in \mathbb{R}^{n_\mu \times s_\mu}$:

$$\mathcal{T}[i_1, \dots, i_d] = \sum_{j_1, \dots, j_d} \mathcal{C}[j_1, \dots, j_d] U_1[i_1, j_1] U_2[i_2, j_2] \dots U_d[i_d, j_d]. \quad (34)$$

If the columns of every U_μ are orthonormal, an effective way to obtain a TT approximation of \mathcal{T} is to first approximate the core \mathcal{C} and then contract the resulting TT with the factor matrices; see, e.g., [Shi et al., 2021]. While orthonormality can always be ensured by computing QR decompositions of the factor matrices, the resulting updates of the core tensor come at a cost of $O(ds^{d+1})$ and typically destroy all sparsity structure in \mathcal{C} . Sketching \mathcal{T} directly avoids these disadvantages and comes with further benefits; for example, its linearity allows us to combine tensors with different types of structure.

We agains use left/right TT DRMs with cores A_1, \dots, A_d and B_1, \dots, B_d , respectively, for sketching a tensor in Tucker format. The sketches Ω_μ and Ψ_μ for a Tucker tensor \mathcal{T} are computed according to the following tensor diagrams:



Carrying out the multiplications $B_{\leq \mu}^\top(U_1 \otimes \cdots \otimes U_\mu)$ and $(U_{\mu+1} \otimes \cdots \otimes U_d)^\top A_{> \mu}^\top$ within the TT format takes $O(dnr^2s)$ flops. The subsequent explicit computation of these matrices by carrying out the contractions in a suitable order requires $O(r^2s^{d-1})$. The cost of computing each of the sketches Ω_μ and Ψ_μ is bounded by $O(rs^d + r^2s^{d-1} + nr^2s)$. This gives a total cost for sketching the Tucker representation using TT DRMs of $O(d(nr^2s + rs^d + r^2s^{d-1}))$.

5 Numerical experiments

In the following, we compare STTA numerically with the classical TT-SVD algorithm and the TT-HMT method mentioned in the introduction. The TT-SVD method is used as baseline since it usually has the smallest approximation error for a fixed rank. The method is however very costly since it requires truncated SVDs of large matricizations. It is also not streamable and less suited for large structured tensors.

STTA and TT-HMT on the other hand are designed for larger tensors. While both methods have similar flop counts for *dense* tensors, TT-HMT does not support streaming and is difficult to implement efficiently in a distributed setting. In its standard formulations of [Huber et al., 2017, Wolf, 2019, Che and Wei, 2019], TT-HMT is also not well suited for structured tensors (but we present a reformulation in the next section that partly alleviates this).

When varying the TT rank in the experiments, we increase it uniformly among all modes whenever possible. At the left/right borders of the TT, the TT ranks may be constrained by the size of the tensor: Given a prescribed rank r we set $r_1 = \min\{r, n_1\}$, $r_{d-1} = \min\{r, n_d\}$, and so on. Unless noted otherwise we set $r_\mu^L = 2r_\mu^R$ for the STTA method, where r_μ^L and r_μ^R are the rank of the left and right DRMs X_μ and Y_μ ; see (12). Since STTA and TT-HMT involve random quantities, we perform 30 trials and show the spread between the 20th and 80th percentile of the relative error $\|\mathcal{T} - \tilde{\mathcal{T}}\|_F / \|\tilde{\mathcal{T}}\|_F$ for the computed approximation \mathcal{T} .

A Python implementation of STTA and the code to reproduce all the experiments is freely available at <https://github.com/RikVoorhaar/tt-sketch>.

5.1 Baseline method TT-HMT

We recall how the HMT method can be used for sketching tensors leading to what we call the TT-HMT method, summarized in Algorithm 5.1. This algorithm produces the same approximation as the algorithms proposed in [Huber et al., 2017, Wolf, 2019, Che and Wei, 2019]. An important numerical and implementation difference is that Algorithm 5.1 continues to operate on the original tensor \mathcal{T} whereas the other algorithms successively reduce the size of \mathcal{T} , like the TT-SVD method. The benefit is that our formulation can exploit structure in \mathcal{T} since only the original \mathcal{T} needs to be accessed during the algorithm.

Superficially TT-HMT method is very similar to the STTA method. However, instead of performing a two-sided sketch using two independent DRMs X_μ and Y_μ , the sketches Ψ_μ on line 4, 6 and 8 in Algorithm 5.1 are computed using only a right DRM X_μ and on the left we multiply by the partial contraction $C_{\leq \mu-1}$ of the TT-cores previously computed. Effectively, this partial contraction $C_{\leq \mu-1}$ can be viewed as a non-random left TT-DRM, and therefore the sketches Ψ_μ can be computed for any of the structured tensors mentioned in Section 4. Note that the TT-HMT method is not streamable due to the orthogonalization on line 11, and requires at least d passes of the data. Furthermore this means it is not possible to parallelize the for loop starting on line 1. On the other hand, the HMT method uses fewer and smaller sketches, making it faster than STTA for smaller rank approximations (for larger rank, this is no longer always true; see Section 5.8), and it also produces orthogonalized TTs. It has a theoretical error bound in expectation with a smaller error constant than STTA; see [Huber et al., 2017].

5.2 Sketching dense tensors

We first consider the problem of sketching dense tensors of shape $n_1 \times \cdots \times n_d$. In particular, we will test the performance of the algorithms on the Hilbert tensor

$$\mathcal{T}_{\text{Hilbert}}[i_1, \dots, i_d] = (i_1 + \cdots + i_d - d + 1)^{-1} \quad (35)$$

and the square-root-sum tensor

$$\mathcal{T}_{\text{sqr}}[i_1, \dots, i_d] = \sqrt{\sum_{j=1}^d \frac{n_j - i_j}{n_j - 1} a + \frac{i_j - 1}{n_j - 1} b}, \quad (36)$$

with $0 < a < b$. Both tensors have exponential decay of the singular values of the unfoldings $\mathcal{T}^{\leq \mu}$ for all μ ; see, e.g., [Hackbusch, 2019]. For \mathcal{T}_{sqr} , the decay worsens as a approaches zero. In our experiments we take $a = 0.2$

Algorithm 5.1 TT-HMT

Input: Tensor \mathcal{T} of shape $n_1 \times \dots \times n_d$; Right DRMs X_μ of size $(n_{\mu+1} \dots n_d) \times r_\mu$.

Output: Cores C_μ of size $r_{\mu-1} \times n_\mu \times r_\mu$ for $1 \leq \mu \leq d$ of a tensor train approximation of \mathcal{T} .

```
1: for  $\mu = 1$  to  $d$  do
2:    $\mathcal{T}^{\leq \mu} \leftarrow \text{reshape}(\mathcal{T}, (n_1 \dots n_\mu) \times (n_{\mu+1} \dots n_d))$ 
3:   if  $\mu = 1$  then
4:      $\Psi_1 \leftarrow \mathcal{T}^{\leq 1} X_1$ 
5:   else if  $\mu < d$  then
6:      $\Psi_\mu \leftarrow (C_{\leq \mu-1}^\top \otimes I_{n_\mu}) \mathcal{T}^{\leq \mu} X_\mu$ 
7:   else
8:      $\Psi_d \leftarrow (C_{\leq d-1}^\top \otimes I_{n_d}) \mathcal{T}^{\leq d}$ 
9:   end if
10:  if  $\mu < d$  then
11:     $C_\mu^L \leftarrow \text{orth}(\Psi_\mu^L)$  // Q factor of QR decomposition
12:     $C_{\leq \mu} \leftarrow (C_{\leq \mu-1} \otimes I_{n_\mu}) C_\mu^L$  // Not formed explicitly
13:     $C_\mu \leftarrow \text{reshape}(C_\mu^L, r_{\mu-1}^L \times n_\mu \times r_\mu^L)$ 
14:  else
15:     $C_d \leftarrow \Psi_d$ 
16:  end if
17: end for
```

and $b = 2$. Furthermore, we take $d = 7$ and $n_1 = \dots = n_7 = 5$ for $\mathcal{T}_{\text{Hilbert}}$, and $d = 5$ and $n_1 = \dots = n_5 = 10$ for $\mathcal{T}_{\text{sqrt}}$. The approximation errors for different TT ranks are shown in Fig. 1 and Fig. 2

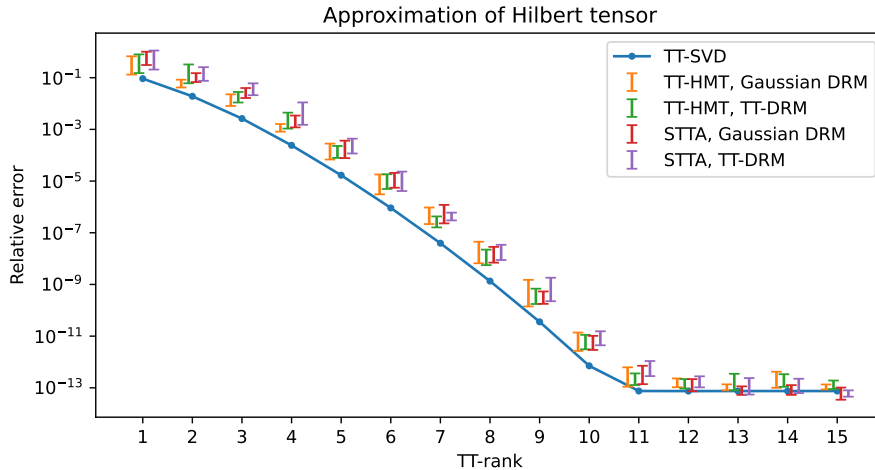


Figure 1: Approximation errors for the Hilbert tensor different TT-ranks for the TT-SVD, STTA and TT-HMT methods. The markers are ordered left-to-right in the same order as the legend.

We observe that the error of STTA and TT-HMT are comparable and only slightly worse than TT-SVD, and has acceptable variance. For both STTA and TT-HMT, there is not much difference between the use of Gaussian and TT DRMs when comparing approximation error and its variance. This is surprising since TT DRMs have less randomness than Gaussian DRMs.

5.3 Sketching a sum of TT and a sparse tensor

One of the major advantages of STTA is that it can approximate the sum of several tensors in parallel, possibly in different formats. As an example we consider the problem of approximating the sum of a low-rank TT and a sparse tensor.

We consider a rank-5 TT of size $(10, 10, 10, 10, 10)$ consisting of cores with i.i.d. $N(0, 1/r^2)$ entries. To this we add a random sparse tensor with 100 nonzero entries. The nonzero entries are normally distributed with standard deviation ranging log-uniformly between 10^{-3} and 10^{-20} . The resulting approximation is shown in Fig. 3.

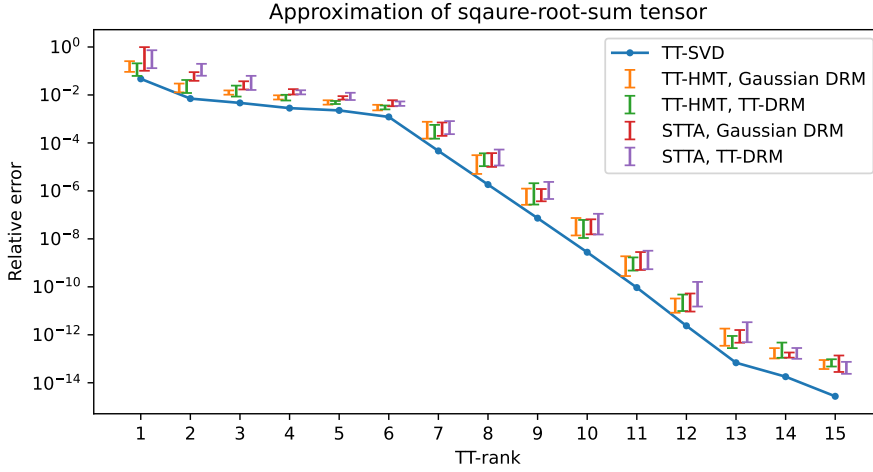


Figure 2: Same setting as in Fig. 1 but for the square-root-sum tensor.

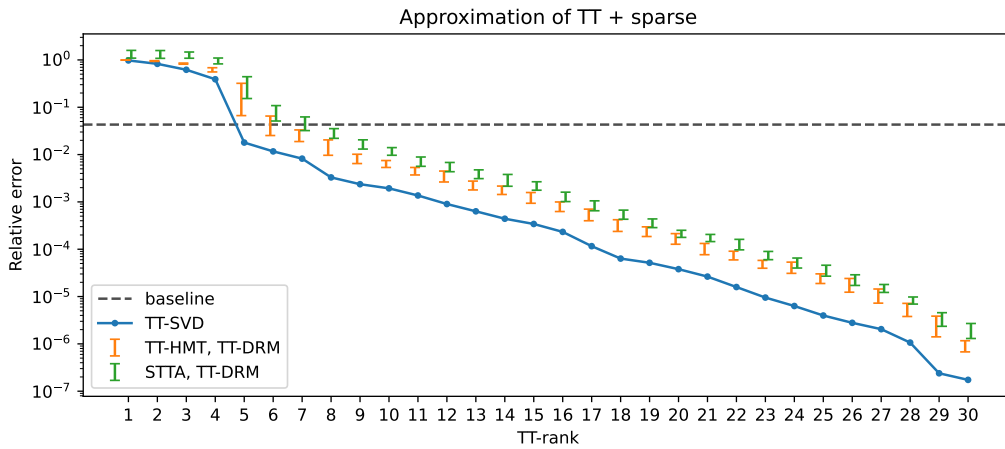


Figure 3: Approximation errors for a sum of a low-rank TT and a sparse tensor for different TT-ranks for the TT-SVD, STTA (right markers) and TT-HMT (left markers) methods. As baseline we show the error obtained when ignoring the sparse tensor and just using the low-rank TT as approximation.

5.4 Sketching a sum of TT

Next we consider the problem of sketching a sum of low-rank TTs. Specifically we take a sum of 20 rank-3 TTs of size $10 \times 10 \times 10 \times 10 \times 10$ of form

$$\mathcal{T} = \sum_{i=0}^{19} 10^{-i} \mathcal{T}_i,$$

where each \mathcal{T}_i is a random TT of rank 3 consisting of cores with i.i.d. $N(0, 1/r^2 n)$ entries. The resulting approximation errors for the different algorithms are shown below in Fig. 4.

5.5 Sketching a CP tensor

We consider the problem of sketching a CP tensor. The CP tensor is of form

$$\mathcal{T} = \sum_{i=1}^{100} \frac{1}{i^5} v_{1,i} \otimes \cdots \otimes v_{5,i},$$

where each $v_{\mu,i} \in \mathbb{R}^{10}$ is a normalized Gaussian vector. The results are shown in Fig. 5.

5.6 The effect of oversampling

The rank r_μ^L of the left DRMs X_μ is required to be smaller than the rank r_μ^R of the left DRMs Y_μ for all μ (or vice versa). Let $r_\mu^R = r_\mu^L + \ell$. We investigate the effect of varying the oversampling $\ell > 0$ on the approximation

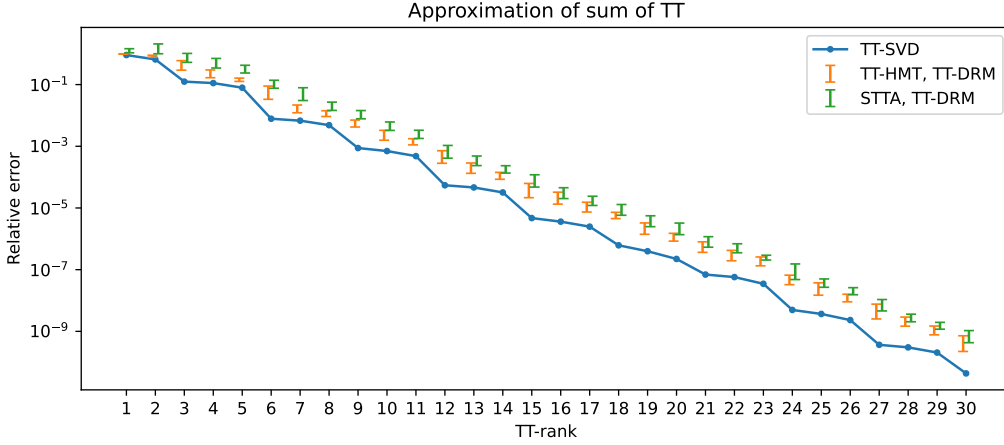


Figure 4: Approximation errors for a sum of a low-rank TTs for different TT-ranks for the TT-SVD, STTA (right) and TT-HMT (left) algorithms.

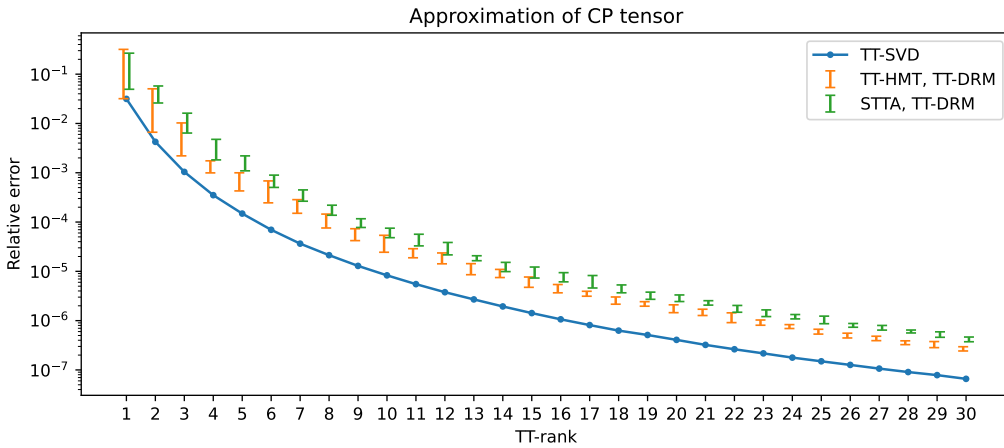


Figure 5: Same setting as in Fig. 4 but for a CP tensor.

error. As test problem we will use the same sum of TTs as in Section 5.4, and we fix the TT rank of the approximation at $r_\mu = r = 10$ for all μ . The result of this experiment is shown below in Fig. 6

Observe that increasing the oversampling ℓ improves both the median and the variance of the approximation error. (Note that the scale for the error in Fig. 6 is logarithmic.) However, in this particular case there are quickly diminishing returns after $\ell \approx 10$. Since the cost of all algorithms depends at most linearly on ℓ , setting $\ell = r$ (as we have done in the experiments above), will only double the computational cost compared to no oversampling at all. This provides a reasonable trade-off between approximation error and speed.

5.7 Dependence of the error on the tensor order

Theorem 3.2 implies that the approximation constant of the STTA method with Gaussian DRMs scales exponentially with the number of modes d . In practice, it appears that the approximation constant scales as $\sqrt{d-1}$ for Gaussian and TT DRMs, like with the classical TT-SVD and the TT-HMT method using Gaussian DRMs. To test this, we compute a rank 10 approximation of a TT of uniform TT-rank $r = 30$ and size 30^d for different values of d . For each unfolding, the TT has singular values decaying exponentially between \sqrt{r} and $\sqrt{r} \cdot 10^{-20}$ (this keeps the Frobenius norm of the TT approximately constant as $d \rightarrow \infty$).

In Fig. 7 we compare the scaling of the approximation error with the tensor order d for TT-HMT and STTA using TT DRMs. We normalize the approximation error by dividing by the approximation error of the TT-SVD method for the same rank. Note that in this context by TT-SVD we mean the standard SVD-based rounding procedure for TTs.

We observe that the STTA method converges to an approximation error roughly 13 times worse than the TT-SVD method, whereas the HMT method converges to an approximation error roughly 8 times worse than the TT-SVD method. This suggests that the approximation constant of the STTA method asymptotically scales

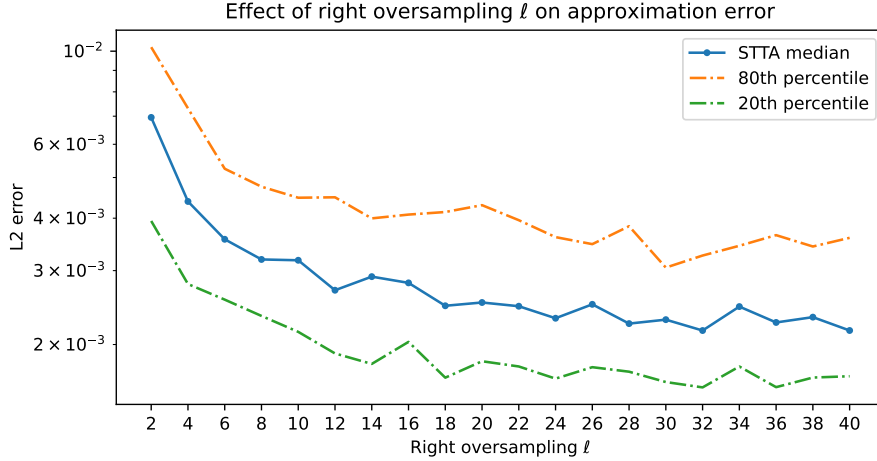


Figure 6: Effect of oversampling parameter $\ell_\mu = |r_\mu^L - r_\mu^R|$ on the approximation error for STTA.

as $\sqrt{d-1}$, just like the TT-SVD and TT-HMT methods.

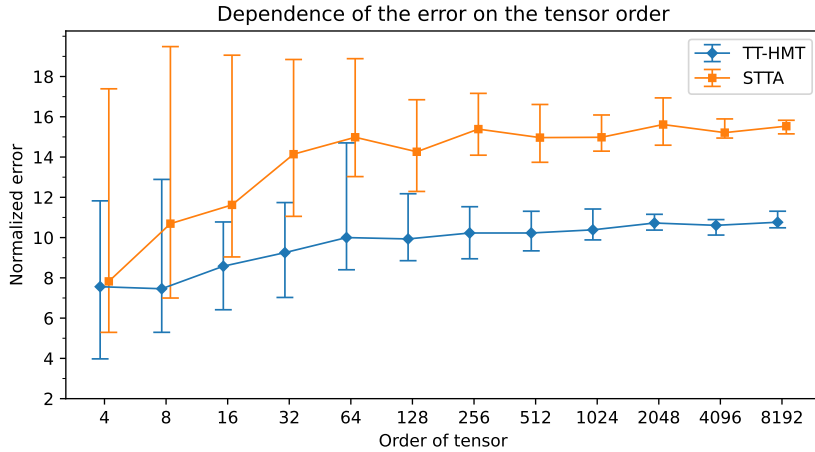


Figure 7: Normalized approximation errors for TTs with varying tensor orders for rank 10 approximations obtained with TT-HMT (left markers) and STTA (right markers). The approximation error is normalized by dividing by the approximation error of the TT-SVD approximation for the same rank.

We remark that the scaling $1/r_\mu^L$ mentioned in Definition 3.3 of TT-DRMs becomes essential for the large number of modes used in this experiment. Different scalings of the cores of the TT-DRMs leads to severe problems with underflow or overflow.

5.8 Timing comparison

We consider the trade-off between speed, rank and approximation error for STTA and the TT-HMT method. In particular we approximate a random TT of size $150 \times 150 \times 150 \times 150 \times 150$ of TT-rank 150. The singular values of each unfolding were made to decay exponentially between 1 and 10^{-10} . In Fig. 8 we report the time taken and relative error of approximation for the TT-HMT and STTA method using TT-DRMs of varying ranks. All experiments were performed on a 2x64 core AMD Epyc 7742. For the approximation error and the time taken we report the median over 100 trials.

While the TT-HMT method is faster for a low-rank approximation, the STTA method is faster than TT-HMT for sufficiently large rank approximations. This is because the cost of the orthogonalization step in TT-HMT becomes dominant for sufficiently large ranks, and offsets the cost of the second sketch in STTA. This is especially true if we use a low amount of oversampling ($r_\mu^L = r_\mu^R + 3$).

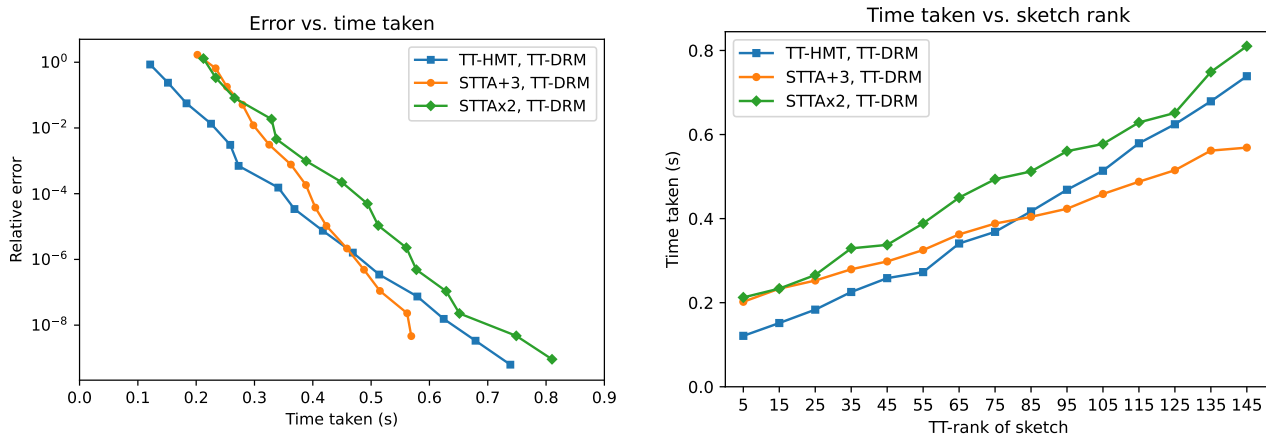


Figure 8: Relation between timing and error (left) and the TT-rank of the TT-DRM and time taken (right) for TT-HMT, and STTA with respectively $r_\mu^L = r_\mu^R + 3$ (STTA+3) and $r_\mu^L = 2r_\mu^R$ (STTAx2).

6 Conclusions

This paper introduced Streaming Tensor Train Approximation (STTA) – an algorithm for approximating a tensor in the tensor train format that is both streamable and one-pass. Since the method computes the approximation using only two-sided sketches of the given tensor, STTA can efficiently update the approximation after linear updates without needing to access the original tensor. In addition, STTA can be applied to specific structures of the tensor such as (linear combinations of) sparsity and various low-rank tensor formats (CP, Tucker, tensor train). In case of sketching with Gaussian dimension reduction matrices and with sufficiently large oversampling, we proved a quasi-optimal error bound in expectation by extending existing results from the Generalized Nyström method for matrices. In addition, the numerical experiments showed that the approximation error concentrates relatively quickly around its mean without needing much oversampling in practice. This is also true when sketching using structured dimension reduction matrices based on tensor trains. Due to the high-level of parallelism, STTA is also faster than computing tensor train approximations based on the Halko–Martinson–Tropp method in a multi-core environment.

References

- [Alger et al., 2020] Alger, N., Chen, P., and Ghattas, O. (2020). Tensor train construction from tensor actions, with application to compression of large high order derivative tensors. *arXiv:2002.06244*. doi:10.48550/arXiv.2002.06244.
- [Bachmayr et al., 2016] Bachmayr, M., Schneider, R., and Uschmajew, A. (2016). Tensor networks and hierarchical tensors for the solution of high-dimensional partial differential equations. *Foundations of Computational Mathematics*, 16. doi:10.1007/s10208-016-9317-9.
- [Che and Wei, 2019] Che, M. and Wei, Y. (2019). Randomized algorithms for the approximations of Tucker and the tensor train decompositions. *Adv Comput Math*, 45(1):395–428. doi:10.1007/s10444-018-9622-8.
- [Clarkson and Woodruff, 2009] Clarkson, K. L. and Woodruff, D. P. (2009). Numerical linear algebra in the streaming model. In *Proceedings of the Forty-First Annual ACM Symposium on Theory of Computing*, pages 205–214. Association for Computing Machinery. doi:10.1145/1536414.1536445.
- [Daas et al., 2021] Daas, H. A., Ballard, G., Cazeaux, P., Hallman, E., Miedlar, A., Pasha, M., Reid, T. W., and Saibaba, A. K. (2021). Randomized algorithms for rounding in the Tensor-Train format. *arXiv:2110.04393*. doi:10.48550/arXiv.2110.04393.
- [Grasedyck et al., 2013] Grasedyck, L., Kressner, D., and Tobler, C. (2013). A literature survey of low-rank tensor approximation technique. *GAMM-Mitteilungen*, 36(1):53–78. doi:10.1002/gamm.201310004.
- [Hackbusch, 2019] Hackbusch, W. (2019). *Tensor Spaces and Numerical Tensor Calculus*, volume 56 of *Springer Series in Computational Mathematics*. Springer Berlin Heidelberg, Berlin, Heidelberg, second edition. doi:10.1007/978-3-642-28027-6.

- [Halko et al., 2011] Halko, N., Martinsson, P. G., and Tropp, J. A. (2011). Finding structure with randomness: Probabilistic algorithms for constructing approximate matrix decompositions. *SIAM Review*, 53(2):217–288. doi:10.1137/090771806.
- [Huber et al., 2017] Huber, B., Schneider, R., and Wolf, S. (2017). A Randomized Tensor Train Singular Value Decomposition. In *Compressed Sensing and Its Applications: Second International MATHEON Conference 2015*, Applied and Numerical Harmonic Analysis, pages 261–290. Birkhäuser, Cham. doi:10.1007/978-3-319-69802-1_9.
- [Khoromskij, 2018] Khoromskij, B. N. (2018). *Tensor Numerical Methods in Scientific Computing*. De Gruyter. doi:10.1515/9783110365917.
- [Kolda and Bader, 2009] Kolda, T. G. and Bader, B. W. (2009). Tensor decompositions and applications. *SIAM Review*, 51(3):455–500. doi:10.1137/07070111X.
- [Ma and Solomonik, 2022] Ma, L. and Solomonik, E. (2022). Cost-efficient Gaussian tensor network embeddings for tensor-structured inputs. *arXiv:2205.13163*. doi:10.48550/arXiv.2205.13163.
- [Nakatsukasa, 2020] Nakatsukasa, Y. (2020). Fast and stable randomized low-rank matrix approximation. *arXiv:2009.11392*. doi:10.48550/arXiv.2009.11392.
- [Orús, 2014] Orús, R. (2014). A practical introduction to tensor networks: Matrix product states and projected entangled pair states. *Annals of Physics*, 349:117–158. doi:10.1016/j.aop.2014.06.013.
- [Oseledets, 2011] Oseledets, I. V. (2011). Tensor-Train Decomposition. *SIAM J. Sci. Comput.*, 33(5):2295–2317. doi:10.1137/090752286.
- [Schollwöck, 2011] Schollwöck, U. (2011). The density-matrix renormalization group in the age of matrix product states. *Annals of Physics*, 326(1):96–192. doi:10.1016/j.aop.2010.09.012.
- [Shi et al., 2021] Shi, T., Ruth, M., and Townsend, A. (2021). Parallel algorithms for computing the tensor-train decomposition. *arXiv:2111.10448*. doi:10.48550/arXiv.2111.10448.
- [Tropp et al., 2017] Tropp, J. A., Yurtsever, A., Udell, M., and Cevher, V. (2017). Practical sketching algorithms for low-rank matrix approximation. *SIAM J. Matrix Anal. & Appl.*, 38(4):1454–1485. doi:10.1137/17M1111590.
- [Uschmajew and Vandereycken, 2020] Uschmajew, A. and Vandereycken, B. (2020). Geometric Methods on Low-Rank Matrix and Tensor Manifolds. In *Handbook of Variational Methods for Nonlinear Geometric Data*, pages 261–313. Springer, Cham. doi:10.1007/978-3-030-31351-7_9.
- [Wolf, 2019] Wolf, A. S. J. W. (2019). *Low Rank Tensor Decompositions for High Dimensional Data Approximation, Recovery and Prediction*. PhD thesis, TU Berlin. doi:10.14279/depositonce-8109.